Applied Physics Letters

Energy storage characteristics of (Pb,La)(Zr,Sn,Ti)O_3 antiferroelectric ceramics with high Sn content

Cite as: Appl. Phys. Lett. **113**, 063902 (2018); https://doi.org/10.1063/1.5044712
Submitted: 15 June 2018 . Accepted: 23 July 2018 . Published Online: 07 August 2018

Yu Dan, Haojie Xu, Kailun Zou, Qingfeng Zhang, Yinmei Lu, Gang Chang, Haitao Huang, and Yunbin He

AIP Publishing

Energy storage characteristics of (Pb,La)(Zr,Sn,Ti)O_3 antiferroelectric ceramics with high Sn content

Yu Dan,[1] Haojie Xu,[1] Kailun Zou,[1] Qingfeng Zhang,[1,a)] Yinmei Lu,[1] Gang Chang,[1] Haitao Huang,[2] and Yunbin He[1,a)]
[1]*Hubei Collaborative Innovation Center for Advanced Organic Chemical Materials, Hubei Key Lab of Ferro and Piezoelectric Materials and Devices, Ministry of Education Key Laboratory of Green Preparation and Application for Functional Materials, Faculty of Materials Science and Engineering, Hubei University, Wuhan 430062, China*
[2]*Department of Applied Physics, The Hong Kong Polytechnic University, Hong Kong, China*

(Received 15 June 2018; accepted 23 July 2018; published online 7 August 2018)

(Pb,La)(Zr,Sn,Ti)O_3 (PLZST) antiferroelectric (AFE) materials have been widely investigated for advanced pulsed power capacitors because of their fast charge-discharge rates and superior energy-storage capacity. For practical applications, pulsed power capacitors require not only large energy density but also high energy efficiency, which are very difficult to achieve simultaneously. To address this problem, we herein investigate the energy-storage properties of PLZST AFE ceramics with a high Sn content by considering that the introduction of Sn can make the polarization versus electric-field (*P-E*) hysteresis loops slimmer. The results show that an optimum Sn content leads to the realization of both large recoverable energy density (W_{re}) and high energy efficiency (η) in a single material. With a Sn content of 46%, the PLZST AFE ceramic exhibits the best room-temperature energy storage properties with a W_{re} value as large as 3.2 J/cm^3 and an η value as high as 86.5%. In addition, both its W_{re} and η vary very slightly in the wide temperature range of 20–120 °C. The high W_{re} and η values and their good thermal stability make the $Pb_{0.97}La_{0.02}(Zr_{0.50}Sn_{0.46}Ti_{0.04})O_3$ AFE ceramic a promising material for making pulsed power capacitors usable in various conditions. *Published by AIP Publishing.*
https://doi.org/10.1063/1.5044712

Today, dielectric capacitors are widely used in radars, lasers, and pacemakers because of their high energy storage density, fast charge-discharge rates, low cost, and good thermal stability.[1–3] Currently, the main materials used in dielectric capacitors are antiferroelectrics (AFEs), ferroelectrics (FEs), linear dielectrics (LDs), and relaxor ferroelectrics (RFEs).[4,5] Among these materials, AFEs have the largest energy storage density because of their double polarization versus electric-field (*P–E*) hysteresis loop characteristics with nearly zero remnant polarization (P_r) and high saturation polarization (P_s). In addition, AFE materials have the fastest charge-discharge rates due to their unique field-induced switching effects during the AFE-FE phase transition.[6–9] As a result, the last few years have witnessed extensive research on (Pb,La)(Zr,Sn,Ti)O_3 (PLZST)-based AFE ceramics.[10–19] For example, Zhang *et al.* used a spark plasma sintering method to fabricate the AFE ceramic $(Pb_{0.858}Ba_{0.1}La_{0.02}Y_{0.008})(Zr_{0.65}Sn_{0.3}Ti_{0.05})O_3$–$(Pb_{0.97}La_{0.02})(Zr_{0.9}Sn_{0.05}Ti_{0.05})O_3$ with a recoverable energy density of $W_{re} = 6.40$ J/cm^3, which is the largest value for bulk dielectric materials reported to date.[20] However, the energy efficiency (η) of this material is only about 62.4%, with the remaining energy transformed to thermal energy. This not only reduces the energy efficiency of the capacitor systems but also affects the material behavior because the heat generated may degrade the energy storage capacity of AFE materials.[21,22] Thus, for practical applications, the AFE material used in capacitors requires not only large energy storage density but also high energy efficiency.

Antiferroelectric materials typically exhibit square-shaped or slim-and-slanted *P–E* hysteresis loops.[23] As shown in our previous work,[18,19] obtaining a slim *P–E* hysteresis loop is the key to the efficiency improvement of pulsed power capacitors. Achieving this objective requires a rational design of the AFE material. A high Sn content induces a more $PbSnO_3$ segregation phase, which leads to thermodynamic instability.[24] This causes inhomogeneity in the chemical composition, which leads to a diffusive AFE-paraelectric (PE) phase transition, similar to the diffuse phase-transition phenomenon in relaxor ferroelectrics.[25] Thus, for PLZST-based AFE materials, a slim *P–E* hysteresis loop may be obtained when the Sn content is high, and hence, high energy density and energy efficiency can be realized simultaneously in the single material. However, to date, the energy storage properties of PLZST AFE ceramics with a high Sn content have not been reported.

We hereby report on the energy storage properties of PLZST antiferroelectric ceramics with a high Sn content. With the optimum Sn content, a large recoverable energy density of 3.2 J/cm^3 and a high energy efficiency of 86.5% are simultaneously obtained in $Pb_{0.97}La_{0.02}(Zr_{0.50}Sn_{0.46}Ti_{0.04})O_3$ AFE ceramics. In addition, the variation of both the recoverable energy density and the energy efficiency in this ceramic is extremely small over the temperature range of 20–120 °C, demonstrating an excellent thermal stability of the energy storage properties. Furthermore, we attempt to correlate quantitatively the energy efficiency with the strain energy (W_{str}) change during the AFE-FE phase transition.

a)Authors to whom correspondence should be addressed: zhangqingfeng@hubu.edu.cn and ybhe@hubu.edu.cn

PbO (≥99%), La_2O_3 (≥99.99%), TiO_2 (≥98%), ZrO_2 (≥99%), and SnO_2 (≥99.5%) (Sinopharm Chemical Reagent Co. Ltd., China) were used as starting raw materials to prepare $Pb_{0.97}La_{0.02}(Zr_{0.50}Sn_{0.39}Ti_{0.11})O_3$ (PLZST 50/39/11), $Pb_{0.97}La_{0.02}(Zr_{0.50}Sn_{0.41}Ti_{0.09})O_3$ (PLZST 50/41/9), $Pb_{0.97}La_{0.02}(Zr_{0.50}Sn_{0.45}Ti_{0.05})O_3$ (PLZST 50/45/5), $Pb_{0.97}La_{0.02}(Zr_{0.50}Sn_{0.46}Ti_{0.04})O_3$ (PLZST 50/46/4), $Pb_{0.97}La_{0.02}(Zr_{0.50}Sn_{0.475}Ti_{0.025})O_3$ (PLZST 50/47.5/2.5), and $Pb_{0.97}La_{0.02}(Zr_{0.475}Sn_{0.525})O_3$ (PLZS 47.5/52.5) AFE ceramics via a conventional solid-state reaction method. The powders were accurately weighed according to the nominal compositions. They are ball milled, dried, and calcined at 870 °C for 2 h, consecutively. The calcined powders were then ball milled again, dried, and pressed into disks. The disks were sintered at 1230 °C for 2 h and polished down to a thickness of 0.2 ± 0.02 mm, which were then brushed with silver paste on both sides and fired at 550 °C for 10 min to obtain the electrodes for electrical property measurements.

The crystal structure of the ceramics was characterized by X-ray diffraction (XRD, D8 Advanced, Bruker, Germany) with Cu Kα radiation. The density was determined by Archimedes' method. The microstructure was observed by scanning electron microscopy (SEM, JSM 6510LV, Jeol, Tokyo, Japan). The *P–E* hysteresis loops were acquired by using a precision ferroelectric measurement system (PolyK Technologies, USA) combined with a high-voltage power supply (Trek 610E; Trek, Lockport, NY, USA) at a frequency of 10 Hz. The energy storage density and energy efficiency were calculated based on the measured *P–E* hysteresis loops.

Figure 1 shows the XRD patterns of the ceramics with various Sn contents measured at room temperature. Only the perovskite phase can be identified in all ceramics with different compositions, and no impurities or secondary phases are detected. In addition, all ceramics show a tetragonal structure, as manifested by the characteristic splitting of the (200) and (002) peaks, as shown in Fig. 1(b). At a fixed Zr content of 50%, with the increasing Sn/Ti ratio, both the (200) and (002) peaks shift to lower angles, indicating the increase in the lattice parameters because of the larger ionic radius of Sn (0.69 Å) than Ti (0.605 Å).

Figures 2(a)–2(f) present the surface morphology of the PLZST ceramics with varying Sn contents, which reveal that all ceramics possess a dense microstructure with an average grain size of about 2–4 μm and no apparent pores on the surface. All ceramics have a high relative density (>97%), as measured by Archimedes' method. This result confirms that the fabricated ceramics are dense, which lays the foundation for obtaining a high electric breakdown strength and a high energy storage density in these ceramics.

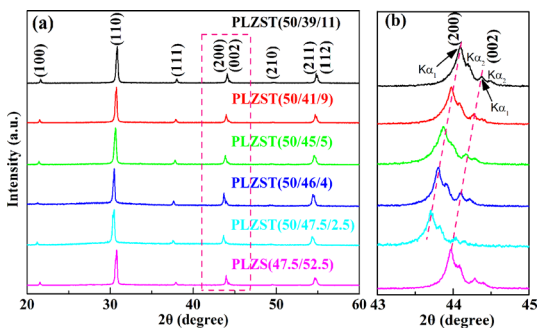

FIG. 1. (a) XRD patterns of PLZST AFE ceramics with Sn contents from 39% to 52.5% sintered at 1230 °C for 2 h. (b) Fine XRD patterns of these ceramics in the 2θ range of 43°–45°; Kα1 and Kα2 denote the diffraction peaks from the Cu Kα1 and Kα2 radiations ($\lambda_{K\alpha1}$ = 1.5406 Å and $\lambda_{K\alpha2}$ = 1.5444 Å), respectively.

Figure 3(a) depicts the room-temperature *P–E* hysteresis loops of the ceramics with various Sn contents at 10 Hz. Based on the hysteresis loops, we obtain the evolution of the AFE-to-FE phase-transition electric field (E_F), the FE-to-AFE phase-transition electric field (E_A), and the electric hysteresis ($\Delta E = E_F - E_A$); P_r, P_{max}, and ΔP ($P_{max} - P_r$); the energy storage density (W) and W_{re}; and η of all ceramics. These data are presented in Figs. 3(b)–3(d). The quantities W, W_{re}, and η are calculated based on the *P–E* loops via the following equations:[14,26]

$$W = \int_0^{P_{max}} EdP \,(\text{upon charging}), \tag{1}$$

$$W_{re} = -\int_{P_{max}}^{P_r} EdP \,(\text{upon discharging}), \tag{2}$$

$$\eta = \frac{W_{re}}{W} \times 100\%, \tag{3}$$

where E, P_{max}, and P_r are the applied electric field, the maximum polarization, and the remnant polarization, respectively. Typical slim-and-slanted double *P–E* hysteresis loops are obtained for all ceramics, confirming the AFE nature of these ceramics. In addition, as expected, the *P–E* loops become slimmer with the increasing Sn content, indicating an increasing energy efficiency. Simultaneously, both E_F and E_A increase with the increasing Sn content, indicating that the AFE phase is stabilized by adding Sn. The phase stability of the perovskite structure (ABO_3) can be evaluated in terms of the tolerance factor t, which is defined as[27]

$$t = \frac{R_A + R_O}{\sqrt{2}(R_B + R_O)}, \tag{4}$$

where R_A, R_B, and R_O are the ionic radii of the A-site cation, B-site cation, and oxygen anion, respectively. In general, when $t > 1$ ($t < 1$), the FE (AFE) phase is stabilized. As mentioned above, the ion radius of Sn is larger than that of Ti. Therefore, when Sn replaces Ti, t decreases, and the AFE phase becomes more stable. In addition, with the Sn content increasing from 0.39 to 0.525, P_{max} decreases from 44.5 to 11.1 μC/cm^2 and P_r decreases from 2.08 to 0.06 μC/cm^2. The spontaneous polarization of ferroelectric materials with an ABO_3 structure is mainly determined by the off-center displacements of B-site ions (Zr^{4+}, Ti^{4+}, and Sn^{4+} for PLZST), O ions, and A-site ions, with larger displacement corresponding to greater polarization.[28] When Sn^{4+} with a larger ionic radius replaces Ti^{4+}, the off-center displacement of the B-site ion is hindered, so that P_{max} decreases. The reduction of P_r is attributed to the improvement of the AFE phase stability. In this work, the highest room-temperature energy storage density W_{re} of 3.2 J/cm^3 is obtained in the $Pb_{0.97}La_{0.02}(Zr_{0.50}Sn_{0.46}Ti_{0.04})O_3$ AFE ceramic with an η value as high as 86.5% benefitting from its large P_{max} and small ΔE.

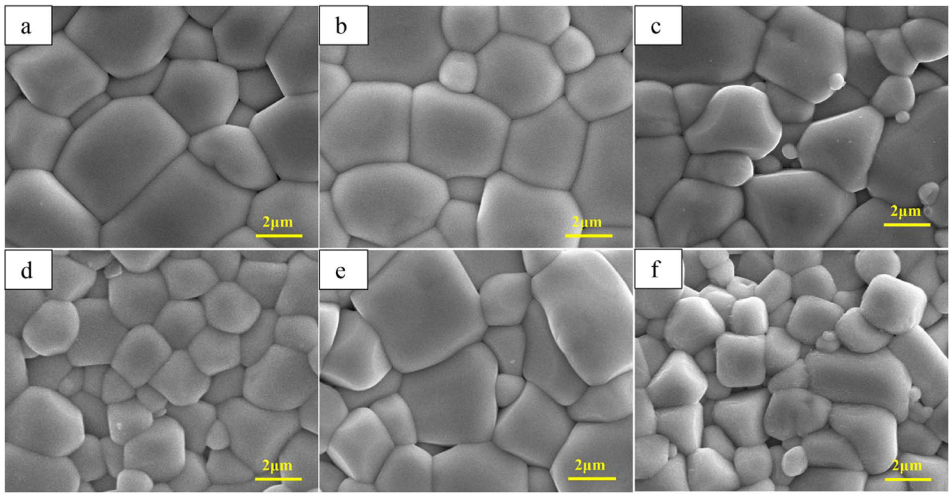

FIG. 2. SEM images of PLZST AFE ceramics with different Sn contents: (a) 39%, (b) 41%, (c) 45%, (d) 46%, (e) 47.5%, and (f) 52.5%.

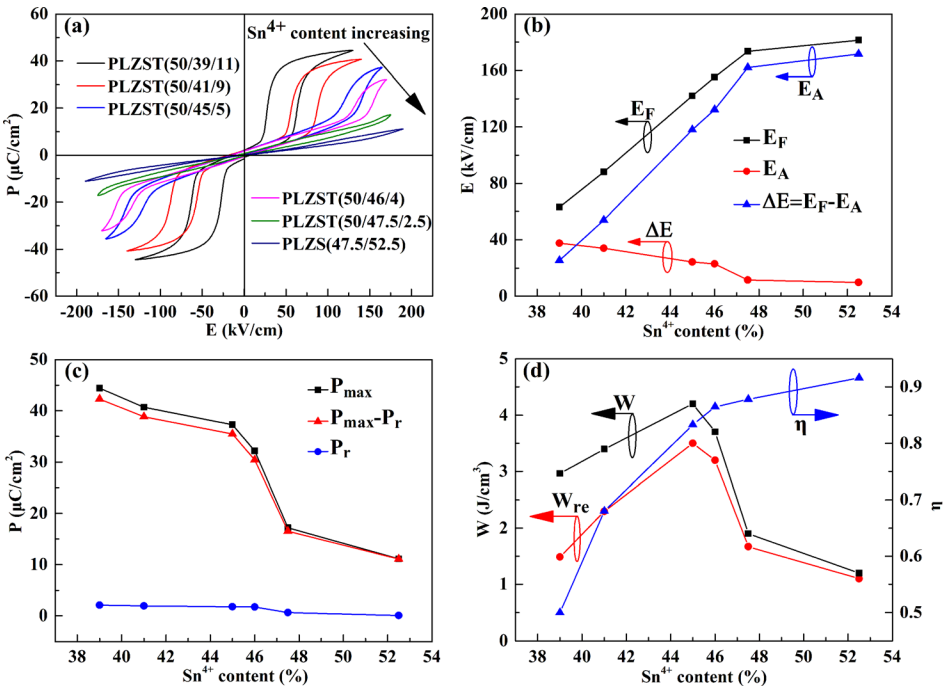

FIG. 3. (a) *P-E* hysteresis loops, (b) E_F, E_A, and ΔE, (c) P_{max}, P_r, and P_{max}-P_r, and (d) W, W_{re}, and η of PLZST AFE ceramics with different Sn contents.

Figure 4 compares the room-temperature W_{re} and η of recently reported PLZST-based AFE ceramics for energy storage applications.[12–15,17,18,20,29–33] Some AFE ceramics exhibit high W_{re} but relatively low η, whereas others possess high η but relatively low W_{re}. In contrast, our high-Sn-content AFE ceramic $Pb_{0.97}La_{0.02}(Zr_{0.50}Sn_{0.46}Ti_{0.04})O_3$ exhibits simultaneously a reasonably large W_{re} and a fairly high η, which makes it overall superior to most lead-based AFE ceramics as demonstrated in Fig. 4 and well comparable with advanced lead-free AFE ceramics, showing the highest W_{re} value of 4.2 J/cm^3 but a low η value of 69%.[34]

In addition to the combination of large W_{re} and high η, the thermal stability of energy storage performance of AFE materials is also important since pulsed power capacitors usually work over a wide range of temperatures for practical applications. Therefore, we have also studied how temperature affects the energy storage performance of our AFE ceramics. Figure 5(a) shows the *P–E* hysteresis loops of PLZST (50/46/4) measured at various temperatures with a maximum electric field up to 150 kV/cm and a fixed frequency of 10 Hz. The temperature dependences of E_F, E_A, P_{max}, P_r, W, W_{re}, and η are summarized in Figs. 5(b) and 5(c). The ceramic exhibits typical AFE double *P–E* hysteresis loops over the temperature range of 20–120 °C, and the *P–E* loops become slimmer with increasing temperature.

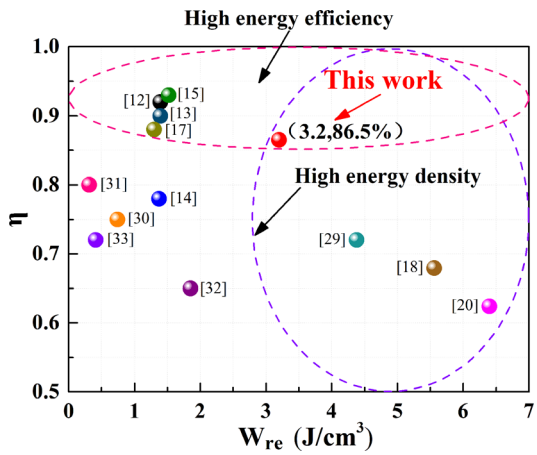

FIG. 4. A comparison of energy densities and efficiencies of recently reported PLZST-based AFE ceramics.

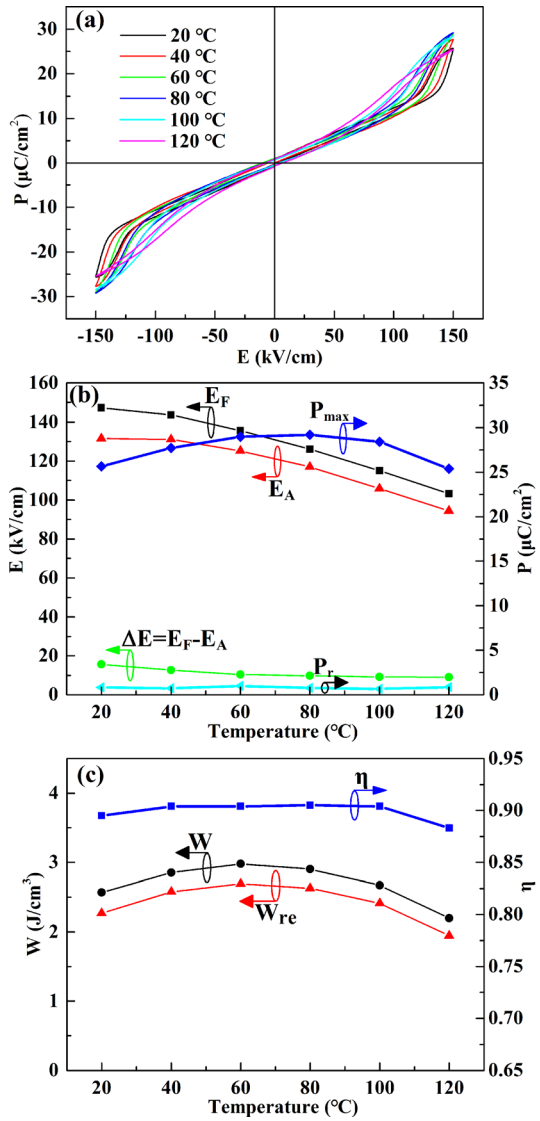

FIG. 5. (a) *P-E* hysteresis loops, (b) E_F, E_A, ΔE, P_{max}, and P_r, and (c) W, W_{re}, and η of the PLZST (50/46/4) AFE ceramic in the temperature range of 20-120 °C measured at a maximum electric field of 150 kV/cm.

This can be attributed to the combined effects of the changing electric dipole interaction energy (W_{inter}) and the strain energy (W_{str}) during the AFE-FE phase transition. The phase transition from AFE to FE requires overcoming the increased electric-dipole interaction energy and strain energy. Thus, E_F is proportional to the sum of the electric-dipole interaction energy and strain energy ($W_{inter} + W_{str}$).[18] The recovery from the FE phase to the AFE phase is caused by the electric-dipole interaction energy that overcomes the strain energy. Therefore, E_A is proportional to the difference between the electric-dipole interaction energy and the strain energy ($W_{inter} - W_{str}$). Thus, ΔE is proportional to twice the strain energy ($\Delta E = E_F - E_A = 2W_{str}$).[18] According to Pan's theory, the strain in the AFE material is derived from the change in the unit-cell volume during the AFE-FE phase transition, which can be expressed as[35]

$$(\Delta V/V) = (\Delta V/V)_F - (\Delta V/V)_A = Q_h \Omega P_{ind}^2, \qquad (5)$$

where Q_h, Ω, and P_{ind} are the electrostrictive coefficient, the coupling coefficient between the antiparallel dipoles, and the polarization induced by the electric field, respectively. The greater the change in the unit-cell volume during the AFE-FE phase transition, the larger the strain in the material. The volumes of the FE rhombohedral, the AFE tetragonal (AFE_T), and the PE cubic (PE_C) phases have the relation: $V_{FE} > V_{PE} > V_{AFE}$.[36] When the temperature increases, the phase transition evolves, as shown in Figs. 6(a) and 6(b), and the volume of the AFE unit cell approaches gradually that of the PE unit cell. Thus, the strain energy decreases and ΔE drops. The maximum polarization P_{max} first increases, reaches the apex at 80 °C, and then decreases with increasing temperature. P_r remains constant over the whole temperature range of 20–120 °C. The reduced ΔE and unchanged P_r, together with the large P_{max}, lead to a large recoverable energy density of 2.7 J/cm^3 and a high energy efficiency of 90.4% at 60 °C. It is known from Fig. 6(b) that the PLZST (50/46/4) ceramic transforms from the tetragonal AFE phase to the cubic PE phase around 150 °C (T_c). In the wide temperature range of 20–120 °C, far below T_c, the AFE phase is quite stable, and thus, W_{re} changes only slightly and η remains around 90% as shown in Fig. 5(c). This indicates that the PLZST (50/46/4) ceramic is a promising candidate for making pulsed power capacitors operable in a wide temperature range.

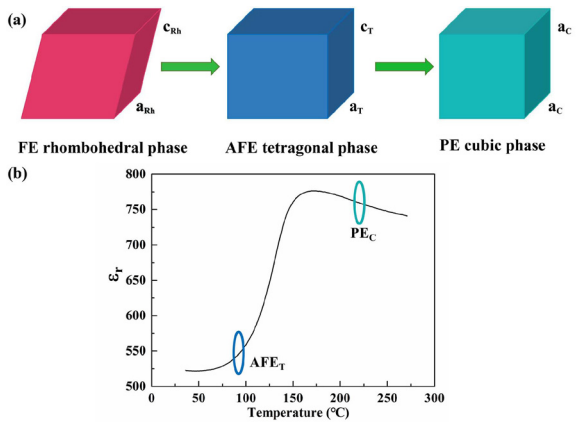

FIG. 6. (a) Schematic diagram of the unit cell evolution of the PLZST (50/46/4) AFE ceramic during the phase transition process. (b) Temperature dependence of the dielectric constant ε_r of the PLZST (50/46/4) AFE ceramic.

In conclusion, PLZST AFE ceramics with a high Sn content in the pure perovskite phase are prepared by using the traditional solid-state reaction method, and the effect of the Sn content on both the energy storage density and efficiency is investigated. With the increasing Sn content, the *P–E* hysteresis loops become slimmer, and the maximum and the remnant polarization decrease gradually. As a result, the energy efficiency η increases continuously, and W_{re} first increases and then decreases. The $Pb_{0.97}La_{0.02}(Zr_{0.50}Sn_{0.46}Ti_{0.04})O_3$ AFE ceramic offers simultaneously a large W_{re} (3.2 J/cm^3) and a high η (86.5%). In addition, its W_{re} and η vary very slightly over a wide temperature range of 20–120 °C. All these results indicate that the $Pb_{0.97}La_{0.02}(Zr_{0.50}Sn_{0.46}Ti_{0.04})O_3$ AFE ceramic is a promising material for application in advance pulsed power capacitors.

This work was supported by the National Natural Science Foundation of China (Grant Nos. 61274010, 51572073,

51602093, and 11774082), the Natural Science Foundation of Hubei Province (Grant Nos. 2015CFA119, 2016AAA031, and 2018CFB700), the State Key Laboratory of Advanced Technology for Materials Synthesis and Processing (Wuhan University of Technology; Grant No. 2018-KF-16), and the Research Grants Council of the Hong Kong Special Administrative Region, China (Project No. PolyU152665/16E).

[1]K. Han, Q. Li, C. Chanthad, M. R. Gadinski, G. Z. Zhang, and Q. Wang, Adv. Funct. Mater. **25**, 3505 (2015).
[2]K. S. Buchanan, X. B. Zhu, A. Meldrum, and M. R. Freeman, Nano Lett. **5**, 383 (2005).
[3]B. J. Chu, X. Zhou, K. L. Ren, B. Neese, M. R. Lin *et al.*, Science **313**, 334 (2006).
[4]B. Li, Q. Y. Liu, X. G. Tang, T. F. Zhang, Y. P. Jiang, W. H. Li, and J. Luo, RSC Adv. **7**, 43327 (2017).
[5]Z. Q. Hu, B. H. Ma, S. S. Liu, M. Narayanan, and U. Balachandran, Ceram. Int. **40**, 557 (2014).
[6]F. Gao, X. Dong, C. Mao, W. Liu, H. Zhang, L. Yang, F. Cao, and G. Wang, J. Am. Ceram. Soc. **94**, 4382 (2011).
[7]Z. Hu, B. Ma, R. Koritala, and U. Balachandran, Appl. Phys. Lett. **104**, 263902 (2014).
[8]Z. Liu, Y. Bai, X. F. Chen, X. L. Dong, H. C. Nie, F. Cao, and G. S. Wang, J. Alloys Compd. **691**, 721 (2017).
[9]Z. Liu, X. Dong, Y. Liu, F. Cao, and G. Wang, J. Am. Ceram. Soc. **100**, 2382 (2017).
[10]R. J. Hwan and S. L. Christopher, J. Appl. Phys. **119**, 024104 (2016).
[11]R. Xu, J. J. Tian, Q. S. Zhu, Y. J. Feng, X. Y. Wei, and Z. Xu, J. Appl. Phys. **122**, 024104 (2017).
[12]R. Xu, B. R. Li, J. J. Tian, Z. Xu, Y. J. Feng, X. Y. Wei, D. Huang, and L. J. Ya, Appl. Phys. Lett. **110**, 142904 (2017).
[13]C. H. Xu, Z. Liu, X. F. Chen, S. G. Yan, F. Cao, X. L. Dong, and G. S. Wang, J. Appl. Phys. **120**, 074107 (2016).
[14]Z. Liu, X. F. Chen, W. Peng, C. H. Xu, X. L. Dong, F. Cao, and G. S. Wang, Appl. Phys. Lett. **106**, 262901 (2015).
[15]R. Xu, Z. Xu, Y. J. Feng, J. J. Tian, and D. Huang, Ceram. Int. **42**, 12875 (2016).
[16]Q. Zhang, X. L. Liu, Y. Zhang, X. Z. Song, J. Zhu, I. Baturin, and J. F. Chen, Ceram. Int. **41**, 3030 (2015).
[17]S. E. Young, J. Y. Zhang, W. Hong, and X. Tan, J. Appl. Phys. **113**, 054101 (2013).
[18]Q. F. Zhang, H. F. Tong, J. Chen, Y. M. Lu, T. Q. Yang, X. Yao, and Y. B. He, Appl. Phys. Lett. **109**, 262901 (2016).
[19]Q. F. Zhang, J. Chen, Y. M. Lu, T. Q. Yang, X. Yao, and Y. B. He, J. Am. Ceram. Soc. **99**, 3853 (2016).
[20]L. Zhang, S. L. Jiang, B. Y. Fan, and G. Z. Zhang, J. Alloys Compd. **622**, 162 (2015).
[21]M. H. Lente and J. A. Eiras, J. Phys.: Condens. Matter **12**, 5939 (2000).
[22]J. Zheng, S. Takahashi, S. Yoshikawa, K. Uchino, and J. W. C. Vries, J. Am. Ceram. Soc. **79**, 3193 (1996).
[23]J. Frederick, X. Tan, and W. Jo, J. Am. Ceram. Soc. **94**, 1149 (2011).
[24]X. F. Chen, Z. Liu, C. H. Xu, F. Cao, G. S. Wang, and X. L. Dong, AIP Adv. **6**, 055203 (2016).
[25]L. E. Cross, Ferroelectrics **151**, 305 (1994).
[26]H. Pan, Y. Zeng, Y. Shen, Y. H. Lin, and C. W. Nan, J. Appl. Phys. **119**, 124106 (2016).
[27]Y. J. Yu and R. N. Singh, J. Appl. Phys. **88**, 7249 (2000).
[28]S. L. Jiang, L. Zhang, G. Z. Zhang, S. S. Liu, J. Q. Yi, X. Xiong, Y. Yu, J. G. He, and Y. K. Zeng, Ceram. Int. **39**, 5571 (2013).
[29]Q. F. Zhang, Y. Dan, J. Chen, Y. M. Lu, T. Q. Yang, X. Yao, and Y. B. He, Ceram. Int. **43**, 11428 (2017).
[30]R. Xu, Z. Xu, Y. J. Feng, H. L. He, J. J. Tian, and D. Huang, J. Am. Ceram. Soc. **99**, 2984 (2016).
[31]H. L. Zhang, X. F. Chen, F. Cao, G. S. Wang, and X. L. Dong, J. Am. Ceram. Soc. **93**, 4015 (2010).
[32]I. V. Ciuchi, L. Mitoseriu, and C. Galassi, J. Am. Ceram. Soc. **99**, 2382 (2016).
[33]R. Xu, Z. Xu, Y. J. Feng, X. Y. Wei, J. J. Tian, and D. Huang, J. Appl. Phys. **119**, 224103 (2016).
[34]L. Zhao, Q. Liu, J. Gao, S. J. Zhang, and J. F. Li, Adv. Mater. **29**, 1701824 (2017).
[35]W. Y. Pan, C. Q. Dam, Q. M. Zhang, and L. E. Cross, J. Appl. Phys. **66**, 6014 (1989).
[36]M. S. Mirshekarloo, K. Yao, and T. Sritharan, Appl. Phys. Lett. **97**, 142902 (2010).